Exploring Drone Utility for Radiation Protection on Martian Ground and Underground

Augustin Tribolet, Crew GreenHab Officer
M.A.R.S. UCLouvain 2023

Abstract

One of the greatest challenges for manned missions to Mars is the high radiation environment that exists in space. Unlike Earth, Mars has a very weak magnetic field and an extremely thin atmosphere, which does not offer sufficient protection against incoming radiation. A promising strategy is to use the Martian ground and underground as a natural shield against such level of radiation. To this end, this project explores the feasibility of using a drone as a valuable tool for locating and analysing potential entrances to the underground. During the maximum activity of the sun, there are extreme solar events that can also contribute to radiation on Mars. In particular, coronal mass ejections unpredictably eject large amounts of energetic particles into space. Under certain conditions, the particles can reach the surface of Mars and could surprise astronauts during an extravehicular activity. The idea here is to use the drone to see how to make the best use of the terrain to be protected from these unpredictable events.

Contents

1. Introduction

M.A.R.S. UCLouvain[1] is an organisation composed of eight students and PhD students affiliated to UCLouvain. Its objective is to build a team for the space analogy mission in the Utah desert (US), the Mars Desert Research Station[2] (MDRS). This desert offers environmental conditions similar to those on Mars. During their stay, participants are responsible for conducting personal scientific experiments that could contribute to space exploration. As part of the M.A.R.S. UCLouvain crew 2023, I present in this report, my experiment conducted inside the station during April 2023, in the MDRS.

The main reason why going to Mars is still not possible is due to the fact that we cannot yet ensure the safety of astronauts. NASA's Human Research Programme has identified five major risks for long-duration missions beyond Earth orbit: radiation, isolation, distance, gravity variations and the spacecraft's hostile environment (1). These missions bring these five risks to another level than on the International Space Station (ISS). In this project, we focus on the radiation exposition on the surface of Mars.

One of the proposal for a Mars mission foresee 6 months to go, 13 months on Mars and 6 months to go back to the Earth (2). Considering the high level of radiation in space, it is difficult to protect astronauts during so long missions. However, on Mars itself, current proposals have highlighted the effectiveness of an underground base (3; 4; 5). Indeed, Mars' past volcanic activities could have left caves and underground structures in its subsurface (6). In this way, it becomes possible to think about getting a radiation-shielded base on Mars. If the on-site part of the mission is guaranteed to be radiation-safe, Mars exploration will only have 12 months left to deal with space radiation. This would be a major step forward.

NASA's recent helicopter on Mars have shown successful experimental flight test, demonstrating rotorcraft flight on Mars (7). Following this result, the idea behind this project is to investigate the use of drone to help astronaut deal with radiation. The aim is to demonstrate drone efficiency in finding a radiation-protected zone by generating Martian landscape model.

This review is organised as follows. Section 2 reviews the radiation effect on the human body, highlighting the importance of the radiation challenges in space. Then in section 3, we recap the main composition of the radiation environment in space we are interested in. In section 4, we present how it is possible

[1] M.A.R.S. UCLouvain, www.marsuclouvain.be
[2] Mars Society, https://mdrs.marssociety.org/

to deal with the different type of radiation using the ground and the underground structure. We present the 3D models generated with the drone and the information that can be extracted for the goal of finding a radiation-shielded site.

2. Radiation effect on human

Due to its extremely thin atmosphere and weak global magnetic field, Mars is not effectively shielded from space radiation. As a consequence, Mars is subject to a powerful particle radiation environment. Exposure to space radiation can lead to four different health risks. It includes an increased possibility of cancer due to the damaging effects of DNA. In addition, prolonged exposure to space radiation can damage the central nervous system, leading to cognitive and neurological disorders. It also causes degenerative effects on various organs and tissues in the body. Finally, acute radiation syndrome (RAS) occurs after short and intense exposure to radiation. This last one can cause immediate fatal symptoms, such as nausea, vomiting and damage to the bone marrow and gastrointestinal system. Figure 1 recaps some of the mean health consequences from exposure to space radiation.

In order to quantify the degree of exposure, astronauts are limited to a dose equivalent (DE, see (3)) exposition during the whole career of 0.47 to 1.47 Sievert (Sv), depending on different factors such as gender and age (8). These dose limits are set to ensure the health and safety of astronauts throughout their careers in space. The NASA design reference mission (2) (360 days in interplanetary space along with 500 days on Mars) corresponds to a DE for the whole mission of 1.01 Sv[3], based on the measurement of the detector RAD on the Curiosity rover (10). We see that the radiation exposure can easily exceed the career dose limit depending on the subject. The contribution of the on-site part only, has been estimated in (11). They found for a 1-year stay on Mars, a total DE of 190.8 to 368.4 mSv depending on the solar activity, see section 3. This DE corresponds to a great portion of the limit for young astronauts, especially for women.

It is therefore essential to mitigate exposure to space radiation on Mars in order to keep astronauts under their DE career limit[4]. Radiation shielding strategies and radiation exposure monitoring are both essential aspects for preserving the health of astronauts on future space exploration missions. DOSTEL instrument aboard of the ISS is an example of device aiming at assessing radiation exposure of astronauts during their space missions (14). More recently, the MARE experiment is studying the effect space radiation on astronaut for the mission

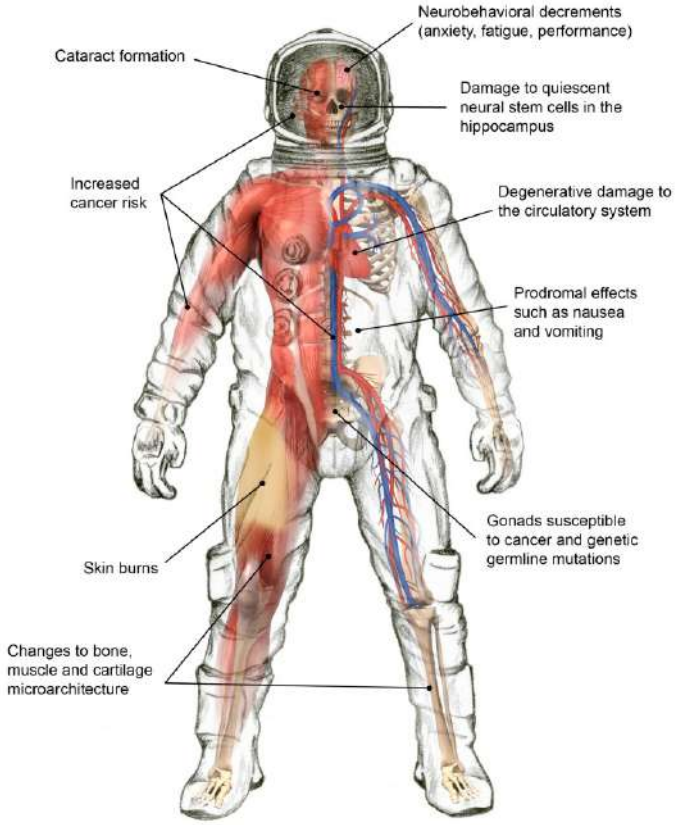

Figure 1: Health consequences resulting from exposure to space radiation. Fig. taken from (8).

Artemis (1). We refer to Thomas Stinglhamber's experiment for radiation monitoring on Mars[5].

3. Space Radiation

In our solar system, we encounter two kinds of radiation component, the Galactic Cosmic Rays and the Solar Particle Radiations. They both contribute to the radiation exposure of astronaut in space and in our case, on Mars. When reaching the atmosphere of Mars, these particles can interact and produce secondary particles. Because the magnetic field of Mars is much weaker and the atmosphere of Mars much tinier than on Earth, primary and secondary particles can reach the soil and even the subsoil of Mars. In particular, the neutrons produced as secondary particles are more challenging to deal with. Indeed, as neutral particle they can penetrate for long distance without interacting (15).

3.1. Galactic cosmic ray

Galactic Cosmic Rays (GCRs) are high-energy particles that originate from outside the solar system and travel through space

[3]For a more concrete comparison, the DOE radiation worker annual limit is set to 20 mSv (9).

[4]Since the new objective to come back to the Moon with the NASA's Artemis program, it is important to note that the limit cited in (2) is subject to change. In addition, radiation exposure on human is still not fully understood. For instance, sex may not be as important as it was tough before, see (12) for more details. Recently, the study (13) has suggested to adopt a universal limit of 600 mSv, with the goal to keep an astronaut below a 3 percent risk of cancer mortality.

[5]Study on Mars Radiation, https://marsuclouvain.be/study-on-mars-radiation/

at nearly the speed of light. They are produced by various astrophysical processes, such as supernova explosions, active galactic nuclei, and other extreme events occurring outside our solar system. These events accelerate charged particles to extremely high energies. GCRs are essentially composed of protons (85 to 90 %), alpha particle (~ 10 to 13 %) (10). The remaining 2% are electrons, neutrons and heavier nuclei.

The energy spectrum of GCRs is very broad, ranging from kiloelectronvolts (keV/nuc) to very high energies of up to 10^{11} GeV/nuc. Another characteristic of GCRs is their relatively constant flux towards the solar system, which is due to the continuous production in the universe. However, these fluxes of charged particles are modulated inside the solar system by the solar activity, which directly impacts the heliospheric magnetic field configuration (16). The GCRS fluxes with energies below a few GeV/nuc are anticorellated with the solar activity, while higher energies are less affected.

Due to their high energies, GCRs can penetrate deep into planetary atmospheres and solid materials, including shields and the surface of Mars. When reacting, they produced a cascade of secondary particles, which drastically increase the level of exposure. As a result, GCRs are difficult to shield against and are the main source of radiation on the surface of Mars and in its subsurface. We are going to focus on them for the problem of long duration shielded habitats on Mars, see section 4.1.

3.2. Solar wind

The solar wind is a flow of high-speed plasma emanating from the outer layer of the Sun's atmosphere, called the corona. This plasma is a mixture of charged particles, mainly electrons and protons, which are expelled from the Sun's outer layers due to the Sun's intense heat and magnetic activity. The Solar Particle Radiation can be divided into two components: the plasma and the Solar Energetic Particles (SEPs). The plasma consists of the low-energy solar wind particles continuously flowing from the Sun, while the SEPs are the highly energetic solar wind particles originating from magnetically disturbed regions of the Sun.

On Earth, the manifestation of photon effects is observed roughly 8 minutes after their emission. The arrival of relativistic energetic particles to the top of the Martian atmosphere takes a similar time, around tens of minutes. In contrast, the impact of plasma requires much more time, typically tens of hours. Mars' magnetosphere and atmosphere are sufficient to stop the lowest energetic particle coming from the sun. So, in this project, we are going to focus on SEPs for which the situation is quite different, see section 4.2.

3.2.1. Strong Energetic Particles

SEPs are bursts of energetic charged particles formed by high-energy processes such as flares and coronal mass ejections (CMEs). They are mainly composed of protons, with a minor contribution of helium ions (around 10%) and heavy ions and electrons (1%). SEP protons and helium ions with energies below 150 MeV/nuc belong to the "soft spectrum" events and are unable to penetrate the Martian surface. For "hard spectrum" events, ions can be accelerated to energies well beyond 150 MeV/nuc. Such particles are able to reach the Martian surface.

The 11-year solar activity cycle is characterised by periods of inactivity during solar minimum, and periods of high activity during solar maximum. In contrast to GCRs, the number of SEPs events is correlated with solar activity. In addition, the most powerful SEPs (several GeV/nuc) are usually seen during solar maximum. The DE received by such SEPs could immediately lead to ADS, discussed in section 2, for astronauts in free space.

3.2.2. Coronal mass ejection

In the context of our Mars project, we are interested in coronal mass ejection (CME) (17; 18). This solar event can indeed have drastic implications for the space environment, see figure 2. CME consists of a massive release of solar wind and magnetic fields from the corona. This phenomenon occurs through the process of magnetic field line reconnection: The magnetic field line may realign into a less tense configuration, due to the Sun's intense magnetic activity.

When a CME occurs, it releases a shock wave of solar material into space (19). This shock wave can accelerate the charged particles it encounters to very high energies, i.e. SEPs. These high amounts of SEPs and magnetic energies can then travel through space and impact planetary bodies. On Earth, such SEPs have already caused damage in the past. They pose radiation hazards to astronauts, satellites, and even passengers on high-altitude flights during strong solar events. On Mars, we encounter the same problems for astronaut and satellite as as well as any robotic missions exploring the planet's surface. CMEs are then of primary concern for future mission towards Mars. In section 4.2, we explore the case of a production of CME towards Mars during the on-site part of a manned Mars mission. Note that future mission to Mars should take place during solar maximum activity to minimise the contribution of GCRs (20). However, the occurrence and intensity of CME increase during solar maximum activity. This underlines the need to consider these unpredictable solar events as possible hazards, and to be prepared to react to them.

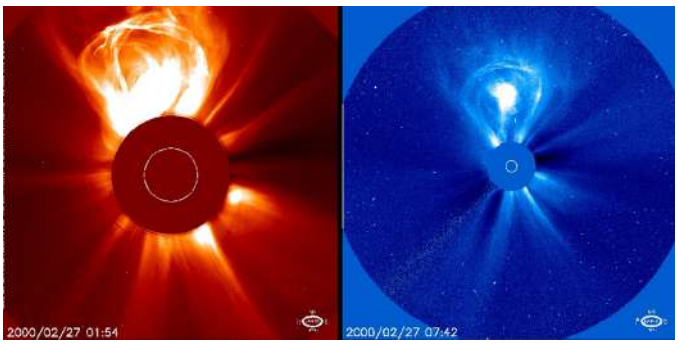

Figure 2: Coronal Mass Ejection on February 27th 2000 observed by the coronagraph of the Solar and Heliosheric Observatory. Credit: SOHO ESA & NASA.

4. Ground and underground protection

Now that we have seen the two components of the radiation present on Mars, we want to see how drones can be helpful in helping astronauts to deal with both of them. As we are going to see below, the ground and the underground are potential solutions. The drone is used to map an area of interest. We used the free software PIX4D Capture to plan, execute, and monitor the drone flights. Then, we can generate 3D models of the ground using photogrammetry. This process begins with the analysis of the images collected by the drones (RealityCapture and DroneDeploy softwares have been used). It first identifies common reference points for the calculations of spatial relationships. It can then reconstruct a 3D model's geometry, which results in a point cloud representing the object's surface, see A.11. Photogrammetry also captures the object's appearance. It maps original images onto the 3D model. The point cloud generated by RealityCapture, for the Marble Ritual region, can be seen in figure A.12. In addition to photogrammetry, DroneDeploy offer different tools to analyse the 3D model. From the original model, topographical map can be we obtained. In figure A.13, we can see the elevation of the North Ridge region and figure A.14 shows the contour lines of the Candor Chasma canyon. DroneDeploy allows also surface and volume measurements.

4.1. GCRs and underground protection

Let's first consider the case of GCRs. As the primary particles are penetrating the atmosphere of Mars, they start to interact and to produce secondary particles. As a consequence, the level of radiation exposure increases as we approach the surface of Mars. In addition, near the surface, particles reflected by the ground contribute to the increase in the radiation level. On figure 3, we can see the evolution of the equivalent dose (ED, see (3)) with the altitude. Surprisingly, the ED is maximum at a depth of 30 cm below the surface. This is due to the remaining primary particles, that have not lost sufficient energy through the atmosphere, that are forced to generate secondary particles when encountering the regolith. In particular, the production of neutron increases drastically the ED (3). On figure 3, we can see that bellow 1 meter, the regolith provides already a good protection against GCRs. The current estimate of natural radioactivity on Mars is about 1 mGy/day. It indicates that GCRs are no longer the main source of radiation below a depth of about 3 metres. Consequently, the effectiveness of protective materials derived from Martian regolith does not improve beyond a thickness of around 3 metres (2; 3). Note that during solar maximum activity, the depth required for radiation protection decreased, see (3).

The observation of Mars has already shown the existence of cave skylights. In (6), they found the presence of entrance of diameter of 100 to 225 m. So it should be possible to find caves in the subsurface of Mars. In addition, lava tubes and cave-like features have been identified through orbital imagery and remote sensing data (5). So both of these structures can be potentially used for radiation protection (3; 4).

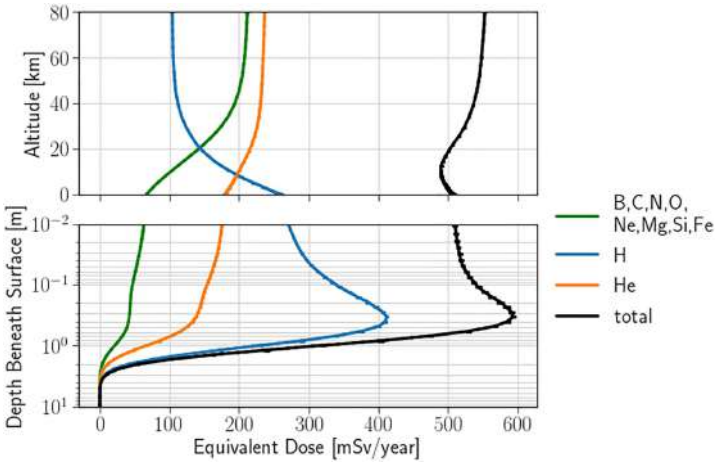

Figure 3: Contribution of the primary particle species to the equivalent dose in a water sphere: hydrogen in blue, helium in orange and heavier primary particle species in green. Fig. taken from (3).

Ground mapping

The 3D model generated with the drone can be used to find potential entrance to the underground. On April 6th and April 12th, the drone has been deployed in the Camel Ridge region, in the South of the station. The 3D model is visible in figure A.21. This is the only area where skylight entrances were detected during the mission, see figures 4, A.17 and A.18.

With photogrammetry, it is also possible to estimate volume. For the research of skylight cave, it could be a powerful tool to estimate the potential of a site for an underground base. We have applied the DroneDeploy tool to the 3D model of the MDRS shown in figure A.16. The volume of the main module is of $\sim 330m^3$. In figure A.19, the volume below the first entry's elevation is represented in blue (it corresponds to fill the model below the reference level, the entry here). The volume found is 6.85 m^3. Of course, the model is not precise enough and it does not represent the real volume. The interior of the caves can in fact be also mapped with photogrammetry (it could also be done with the drone, see section 5 for more details). In this case, it means that we could estimate the volume of a cave and its potential for an underground base.

Having the cave's depth in the underground, one could also estimate the amount of material above a given level inside the cave. In figure A.20, the amount of material above the second entry is estimated to $\sim$ 4801 m^3, in red. Geant4 could be used to predict the level of radiation inside a cave providing the 3D structure, assuming the regolith composition and the type of radiation involved. In other words, we could estimate the effectiveness of a cave in absorbing radiation.

4.2. CMEs and ground protection

In ref. (11), it was shown that ground levels with lower altitude have a reduced level of radiation. This is easily understood as lower altitude leads to a better shielding effect from the at-

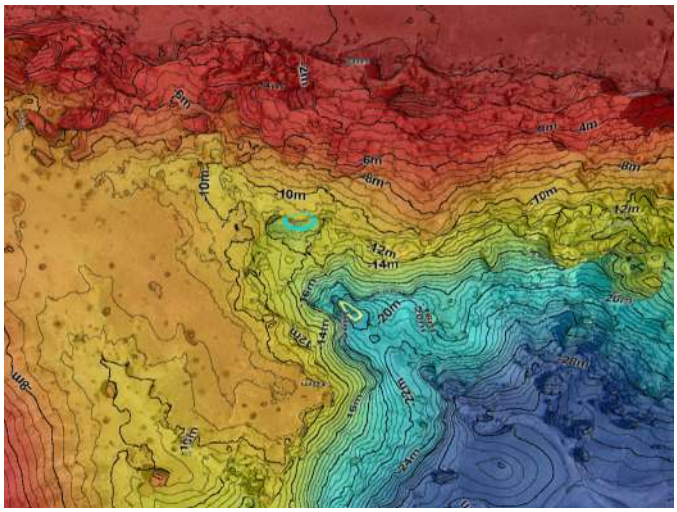

Figure 4: Skylight caves identified in the Kissing Camel Ridge region, in light blue and yellow.

mosphere[6]. The surface of Mars is covered by high mountains and low-altitude craters, so that the atmosphere thickness can vary by a factor 10 in this range of altitudes (15). In figure 5, we can clearly see the typical Martian topography and the corresponding elevation variation.

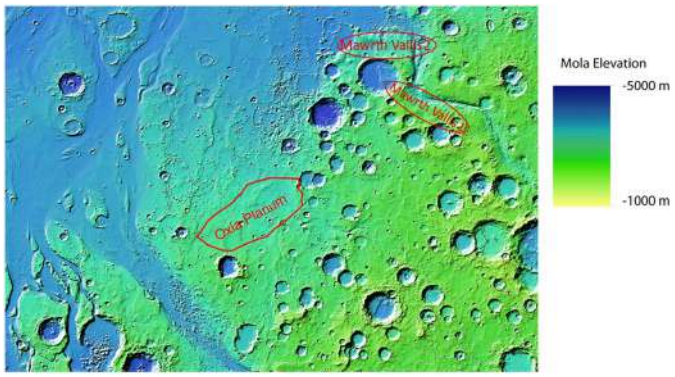

Figure 5: Topographical map of Mars generated by the Mars Orbiter Laser Altimeter (MOLA). Fig. taken from (11).

On Earth, the arrival of CMEs is first monitored by the Deep Space Climate Observatory (DSCOVR) satellite. A CME can be first detected by the sudden emission of X-Rays and radio wave emission from the sun. When these electromagnetic signals are detected, it can provide some time to react before the arrival of the SEPs: 15 to 60 minutes depending on their energies. The solar plasma, propagating much slower, can arrive

[6]Note that the behaviour of the radiation approaching the surface is the same as that discussed above, see figure 3, but with a weaker ground level radiation due to the increase of shielding effect. Remarque in addition, that a given site can have daily fluctuation in the radiation level. Indeed, in (10), it was shown that daily variation in atmospheric pressure and total dose rate are anticorellated.

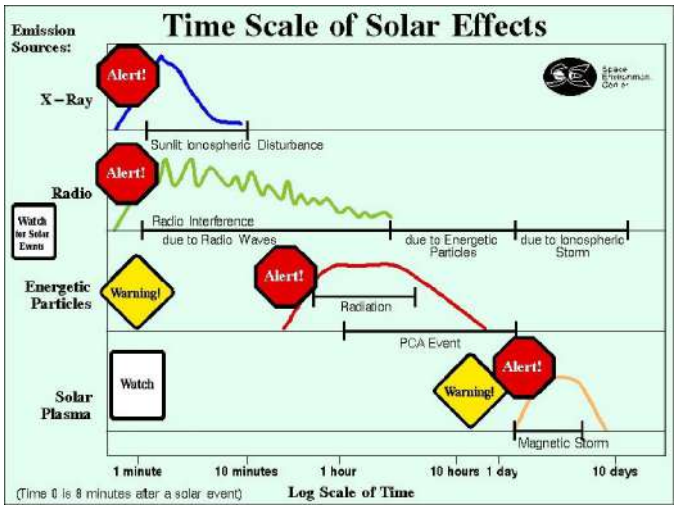

Figure 6: Example of a typical time scale for a coronal mass ejection reaching the Earth. Electromagnetic waves are the first to reach the Earth, signalling the emission of a CME. They are followed shortly by energetic particles, and much later by solar plasma. Fig. taken from (21).

much after, after around 15h (17). On figure 6, we can see the time scale of a CME reaching Earth. SEPs are going to increase the radiation reaching Earth, while the subsequent plasma can cause magnetic storms. Also, the huge flow of magnetic energies contract the magnetic field reducing the protection of Earth against radiation.

Note that the Two-Way Communication Time between Earth and Mars vary from 6.3 to 44.5 minutes (2). It is therefore important that future astronauts on Mars can be autonomous in the detection of such event. We can imagine such a proper satellite like DSCOVR for the astronaut on Mars. As on Earth, they then have between 15 to 60 minutes to minimise the risk of radiation exposure. As seen before, they have several options. The Martian atmosphere can better shield SEP events since they usually contain lower energy particles than GCRs (22). This means that when dealing with CMEs, astronauts can already have a good protection using the great variability of the thickness of the atmosphere, see figure 5. In addition to being at a lower altitude, enclosed environments with cliffs, such as canyons and craters, have a reduced angle of view and are therefore less exposed to radiation. Going in the underground gives the best protection, but it is unlikely to find an easy entry in such a short interval of time. As a consequence, when dealing with CMEs, we will analyse the topography of the 3D model in order to quickly react.

Itinerary planning

On 08th April 2023, the Special Region and the Lith Canyon have been mapped. The 3D model reconstructed is given in figure A.24. If we consider the case of a CME, one need to find the lowest altitude in the local environment. The map can be used to find the most appropriate way to reach it. In figure 8, we have envisaged two ways to join the canyon, with the lowest altitude (around 1344 m): One with the most direct way,

and one with a deviation to the East.

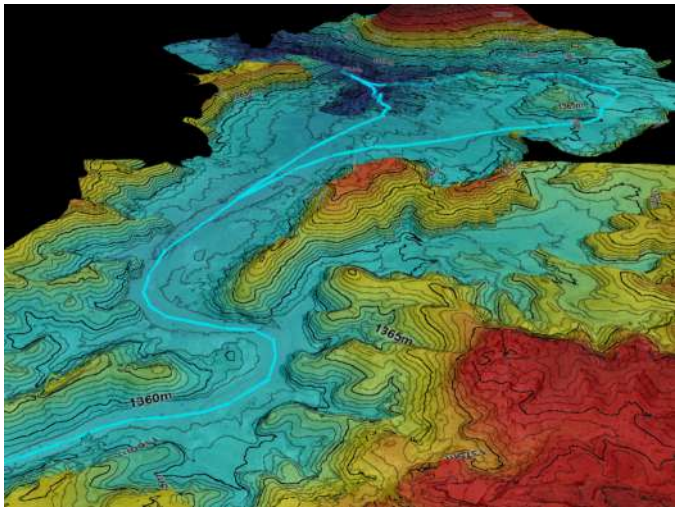

Figure 7: Planned routes to reach the radiation-shielded canyon site in the north, starting from the southern position.

Figure 8, represents the elevation profiles of both of the path. The average slope can be roughly estimated for the two paths. For the first path, the stiff descent to the Lith Canyon is spread over 100 m for an altitude difference of 12 m. This gives an average slope of 0.12. While the second one, is spread over 260 m for 17 m. So that, the smoothest way is the second path, with an average slope of 0.065. If one is confronted to CMEs, the route will be chosen depending on how we can reach the canyon. If the astronauts are equipped for climbing, the shortest route should be considered. Otherwise, if the astronauts have a rover, the second route is certainly more efficient for reaching the canyon.

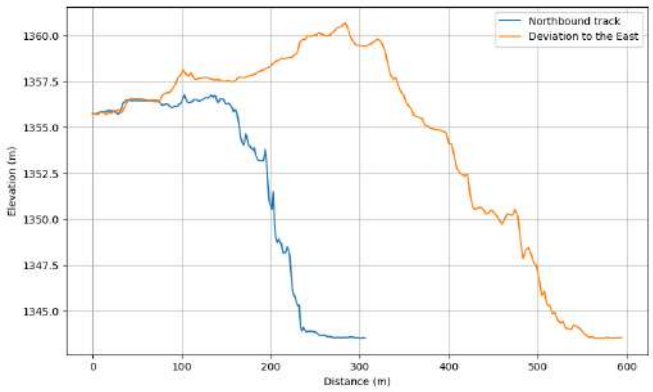

Figure 8: Elevation profiles for the northern road, in orange, and eastern road, in blue. One can see that the average slope is less steep for the eastern path.

4.3. The presence of water

In their paper (3), they also found that the presence of water in the composition of the soil can drastically change the protection against radiation. On figure 9, we can see that a 50% and 10% water composition reduces the ED at the surface level by 45% as compared with the previous dry scenario[7]. In the context of finding a radiation-protected site during the arrival of a CME, we also need to look for a water-rich regolith, in addition to the low-altitude criteria. Going further in depth, we can also see the effectiveness of water-rich soil to enhance the regolith's radiation protection. Consequently, long-term underground bases should be installed in water-rich areas.

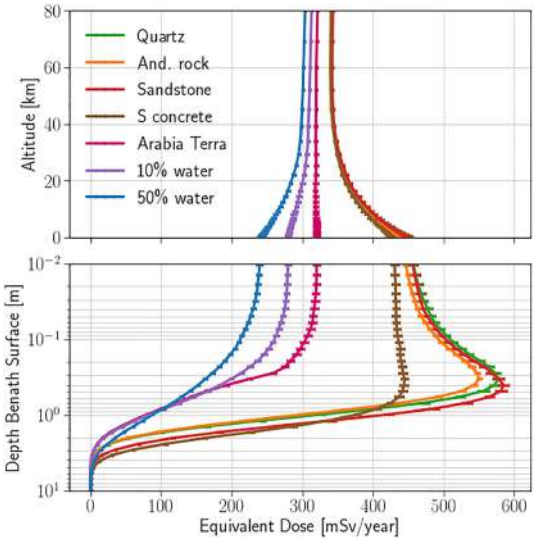

Figure 9: Equivalent dose in a water sphere as a function of atmospheric and Martian regolith depth for different regolith composition. Fig. taken from (3).

The presence of water on the pole of Mars was already known. On December 2024, NASA's Insight mission observed a meteorite impact on the equator of Mars. The satellite observation detected pieces of ice excavated from the soil, showing the presence of water at the equator level (23). Nasa's Mars EXPRESS mission also detected a large reservoir of liquid water deep beneath the surface of Mars (22). In addition, in the article (24), it was shown that a large quantity of water could have been fixed in the crust of Mars by interacting with minerals. All these results show that the presence of water in regolith can indeed be taken into account in the search for a radiation-protected zone. The radiation reflected and absorbed provides a better shield both above and below the surface.

Surface measurement

On 13th April 2023, we have investigated the region of the Cowboy Corner, around Monte Tharsis. The 3D model reconstructed is given in figure A.27. In this area, a water surface has been identified, see figure 10 in light blue. The measurement of the area on the model gives around 54 m^2, see figure A.26. Of course, on Mars, such open liquid surfaces are not present. To detect ice, drone could be equipped with spectral camera.

[7]This is explained by a drastic reduction of the upward flux of low energy neutrons, which contains the most biologically impacting neutrons (at 1 MeV). Indeed, the presence of hydrogen makes neutrons lose energy more efficiently which can then be captured by hydrogen producing gamma rays, see (3) for more details.

In this case, one may estimate the amount of water present in the regolith, while the surface area containing the water-rich regolith could be estimated with the 3D model.

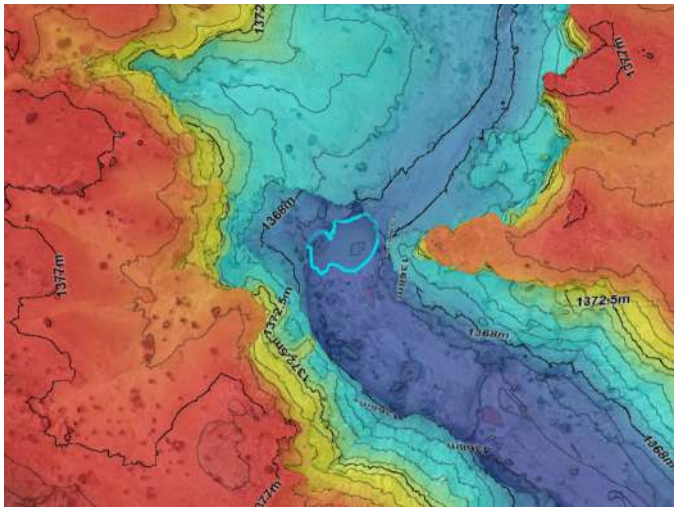

Figure 10: Water surface area identified in the nearby region of Monte Tharsis 3D model.

5. Outlook

In addition to the radiation protection benefit, the underground structures also provide several advantages for human habitation on Mars. Mars experiences extreme temperature variations, with average temperatures well below freezing. Therefore, underground structures can help mitigate this high range of extreme temperatures. In addition, Mars is known for its frequent dust storms (25), which can pose risks to equipment and human health. Underground structures offer a natural barrier against the impact of these storms. Moreover, natural caves and rock formations have already undergone millions of years of geological processes, making them structurally stable. This stability provides a secure foundation for developing and expanding underground habitats (4).

In this article (5), lava tubes were investigated as possible locations for biological signatures. In other words, when looking for sites protected from radiation, we also find sites that are most likely to present biological signatures, see also (26) for more details. We refer to Agnès Dekeyser's experiment for the Martian biological signatures[8].

It is important to note that the photogrammetry method used in this project requires the use of GPS telemetry. Such systems do not exist on Mars. However, the LIDAR camera can be used as an independent and powerful alternative for 3D mapping. LIDAR reconstructs 3D scenes using the reflection of laser light. Tools have already been developed to get a 3D map generated in real time.

Finally, we refer to the previous work done on cave exploration as solution to radiation protection. See in particular the complementary project, pursued by the SETI Institute and Astrobotic Technology[9], of using drones directly inside caves to scan the interior in 3D. As well as, the CHILL-ICE Analogue Astronaut Mission[10] which explored the fast installation of an underground based, in a lava-tube, just after the landing of a manned Martian mission.

6. Conclusion

Radiation is one of the main problems for space exploration. In this work, we investigated the possibility of using drones to help astronauts finding radiation-protected sites on Mars. We found several advantages in using them to deal with GCRs and SEPs.

GCRs have a constant flux and can reach very high energies. For these reasons, they are the main source of radiation and are difficult to shield against. Mars' underground structures provide a natural shield below a depth of at least one meter. During the simulation, 3D reconstruction generated by photogrammetry enabled us to find two skylight cave entrances in the Kissing Camel Ridge area. The 3D model was used to estimate the volume at the entrance of the first cave and the amount of material above the second entrance level. It can also be used to measure specific volume, and we applied it to the MDRS main module.

Mars' atmosphere and magnetosphere offer good protection against the solar particles. However, this is not the case for SEPs, with higher energies. The case of CMEs towards Mars was considered as a second part of the project. The fast propagation of SEP does not give astronauts a lot of time to react. Low-altitude sites, with higher atmospheric column depths, offer better protection against these events. In addition, enclosed sites also reduce incoming radiation, making canyons and craters ideal locations in the case of an incoming CME. In this scenario, we used drones to study the special region. The lowest altitude and the most enclosed environment were identified using the topographic map generated: the Lith Canyon. Two possible routes were then considered to reach this lowest altitude. Using the 3D model, we concluded that the easiest way to reach the bottom of the canyon was the most direct route if climbing equipment was available, and the eastern part, with the smoothest route, if not.

Water-rich sites can enhance surface and subsurface projection. This is due to the radiation reflected and absorbed by the water-rich regolith. The generated 3D model can be used to estimate surfaces. It has been applied for the 3D model around Monte Tharsis, to highlight the advantage of surface measurement for estimating the surface of water-rich sites.

[8]Study on the Capacity of Extremophiles to Adapt Under Mars' Extreme Conditions: https://marsuclouvain.be/study-on-the-capacity-of-extremophiles-to-adapt-under-mars-extreme-conditions/.

[9]Drone Maps Icy Lava Tube in Iceland in Preparation for Cave Exploration on the Moon and Mars: https://www.seti.org/press-release/drone-maps-icy-lava-tube-iceland-preparation-cave-exploration-moon-and-mars/.

[10]Construction of a Habitat Inside a Lunar-Analogue Lava-tube, https://euromoonmars.space/Chillice/main/

Acknowledgements

First of all, I would like to warmly thank Véronique Dehant and Viviane Pierrard for guiding me for the scientific context of the project. My deepest gratitude to Bernard H. Foing and Jérôme Loicq for their comments and suggestions for the development of the project. Many thanks to Olivier Boissard, Julien Vandanjon and Sébastien Lambot for their valuable advices on drone operations and photogrammetry processes.

My thanks also to our project partners for their support[11], which allowed the acquisition of the drone. In particular for this project, a special thanks to EspaceDrone[12] for giving me the opportunity to attend a drone piloting training session, RealityCapture[13] and DroneDeploy[14] for generously providing me access to their photogrammetry software, and finally to Objet Témoin for the provision of an efficient computer for photogrammetry[15].

Last but not least, my sincere thanks go to the whole M.A.R.S. UCLouvain 2023 crew for their motivation and continuous support throughout the year, and especially during the simulation. Thank you for this incredible experience.

References

[1] Razvan Gaza, Hesham Hussein, Dave Murrow, Josh Hopkins, Gideon Waterman, Oren Milstein, Thomas Berger, Bartos Przybyla, Joachim Aeckerlein, Karel Marsalek, et al. Matroshka astrorad radiation experiment (mare) on the deep space gateway. *LPI Contributions Journal*, 2018.

[2] Bret G. Drake, Stephen J. Hoffman, and David W. Beaty. Human exploration of mars, design reference architecture 5.0. In *2010 IEEE Aerospace Conference*, pages 1–24, 2010. doi:10.1109/AERO.2010.5446736.

[3] Lennart Röstel, Jingnan Guo, Saša Banjac, Robert F Wimmer-Schweingruber, and Bernd Heber. Subsurface radiation environment of mars and its implication for shielding protection of future habitats. *Journal of Geophysical Research: Planets*, 125(3):e2019JE006246, 2020.

[4] Morteza Sheshpari, Yoshiaki Fujii, and Takuya Tani. Underground structures in mars excavated by tunneling methods for sheltering humans. *Tunnelling and Underground Space Technology*, 64:61–73, 2017. URL: https://www.sciencedirect.com/science/article/pii/S088677981530239X, doi:https://doi.org/10.1016/j.tust.2016.12.015.

[5] Richard J. Léveillé and Saugata Datta. Lava tubes and basaltic caves as astrobiological targets on earth and mars: A review. *Planetary and Space Science*, 58(4):592–598, 2010. Exploring other worlds by exploring our own: The role of terrestrial analogue studies in planetary exploration. URL: https://www.sciencedirect.com/science/article/pii/S0032063309001603, doi:https://doi.org/10.1016/j.pss.2009.06.004.

[6] G. E. Cushing, T. N. Titus, J. J. Wynne, and P. R. Christensen. Themis observes possible cave skylights on mars. *Geophysical Research Letters*, 34(17), 2007. URL: https://agupubs.onlinelibrary.wiley.com/doi/abs/10.1029/2007GL030709, arXiv:https://agupubs.onlinelibrary.wiley.com/doi/pdf/10.1029/2007GL030709, doi:https://doi.org/10.1029/2007GL030709.

[7] NASA Jet Propulsion Laboratory. Mars Helicopter Status. https://mars.nasa.gov/technology/helicopter/status/.

[8] Jeffery C. Chancellor, Graham B. I. Scott, and Jeffrey P. Sutton. Space radiation: The number one risk to astronaut health beyond low earth orbit. *Life*, 4(3):491–510, 2014. URL: https://www.mdpi.com/2075-1729/4/3/491, doi:10.3390/life4030491.

[9] U.S. Department of Energy (DOE). Doe ionizing radiation dose ranges charts. https://www.energy.gov/ehss/articles/doe-ionizing-radiation-dose-ranges-charts, Accessed 2023.

[10] Donald M Hassler, Cary Zeitlin, Robert F Wimmer-Schweingruber, Bent Ehresmann, Scot Rafkin, Jennifer L Eigenbrode, David E Brinza, Gerald Weigle, Stephan Böttcher, Eckart Böhm, et al. Mars' surface radiation environment measured with the mars science laboratory's curiosity rover. *science*, 343(6169):1244797, 2014.

[11] F Da Pieve, G Gronoff, J Guo, CJ Mertens, L Neary, B Gu, NE Koval, J Kohanoff, AC Vandaele, and F Cleri. Radiation environment and doses on mars at oxia planum and mawrth vallis: Support for exploration at sites with high biosignature preservation potential. *Journal of Geophysical Research: Planets*, 126(1):e2020JE006488, 2021.

[12] Karen Krukowski, Katherine Grue, Elma S. Frias, John Pietrykowski, Tamako Jones, Gregory Nelson, and Susanna Rosi. Female mice are protected from space radiation-induced maladaptive responses. *Brain, Behavior, and Immunity*, 74:106–120, 2018. URL: https://www.sciencedirect.com/science/article/pii/S0889159118304173, doi:https://doi.org/10.1016/j.bbi.2018.08.008.

[13] National Academies of Sciences, Engineering, and Medicine. *Space Radiation and Astronaut Health: Managing and Communicating Cancer Risks*. The National Academies Press, Washington, DC, 2021. doi:10.17226/26155.

[14] Berger, Thomas, Matthiä, Daniel, Burmeister, Sönke, Zeitlin, Cary, Rios, Ryan, Stoffle, Nicholas, Schwadron, Nathan A., Spence, Harlan E., Hassler, Donald M., Ehresmann, Bent, and Wimmer-Schweingruber, Robert F. Long term variations of galactic cosmic radiation on board the international space station, on the moon and on the surface of mars. *J. Space Weather Space Clim.*, 10:34, 2020. doi:10.1051/swsc/2020028.

[15] Jordanka Semkova, Victor Benghin, Jingnan Guo, Jian Zhang, Fabiana Da Pieve, Krasimir Krastev, Yuri Matviichuk, Borislav Tomov, Vyacheslav Shurshakov, Sergey Drobyshev, et al. Comparison of the flux measured by liulin-mo dosimeter in exomars tgo science orbit with the calculations. *Life Sciences in Space Research*, 2022.

[16] L. J. Gleeson and W. I. Axford. Solar Modulation of Galactic Cosmic Rays. , 154:1011, December 1968. doi:10.1086/149822.

[17] Space Weather Prediction Center. Coronal mass ejections. https://www.swpc.noaa.gov/phenomena/coronal-mass-ejections, Accessed 2023.

[18] Jingnan Guo, Xiaolei Li, Jian Zhang, Mikhail I Dobynde, Yuming Wang, Zigong Xu, Thomas Berger, Jordanka Semkova, Robert F Wimmer-Schweingruber, Donald M Hassler, et al. The first ground level enhancement seen on three planetary surfaces: Earth, moon, and mars. *Geophysical Research Letters*, 50(15):e2023GL103069, 2023.

[19] David F. Webb. Coronal mass ejections and space weather. *Proceedings of the International Astronomical Union*, 2004(IAUS223):499–508, 2004. doi:10.1017/S1743921304006696.

[20] M. I. Dobynde, Y. Y. Shprits, A. Y. Drozdov, J. Hoffman, and Ju Li. Beating 1 sievert: Optimal radiation shielding of astronauts on a mission to mars. *Space Weather*, 19(9):e2021SW002749, 2021. e2021SW002749 2021SW002749. URL: https://agupubs.onlinelibrary.wiley.com/doi/abs/10.1029/2021SW002749, arXiv:https://agupubs.onlinelibrary.wiley.com/doi/pdf/10.1029/2021SW002749, doi:https://doi.org/10.1029/2021SW002749.

[21] Heliophysics Virtual Observatory (HELIO). HELIO Science. https://helio-vo.eu/science.php.

[22] R. Orosei, S. E. Lauro, E. Pettinelli, A. Cicchetti, M. Coradini, B. Cosciotti, F. Di Paolo, E. Flamini, E. Mattei, M. Pajola, F. Soldovieri, M. Cartacci, F. Cassenti, A. Frigeri, S. Giuppi, R. Martufi, A. Masdea, G. Mitri, C. Nenna, R. Noschese, M. Restano, and R. Seu. Radar evidence of subglacial liquid water on mars. *Science*, 361(6401):490–493, 2018. URL: https://www.science.org/doi/abs/10.1126/science.aar7268, arXiv:https://www.science.org/doi/pdf/10.1126/science.aar7268, doi:10.1126/science.aar7268.

[23] D. Kim, W. B. Banerdt, S. Ceylan, D. Giardini, V. Lekić, P. Lognonné, C. Beghein, É. Beucler, S. Carrasco, C. Charalambous, J. Clinton,

[11] https://marsuclouvain.be/our-sponsors/

[12] https://www.espacedrone.be/accueil

[13] https://www.capturingreality.com/

[14] https://www.dronedeploy.com/

[15] http://www.objettemoin.org

M. Drilleau, C. Durán, M. Golombek, R. Joshi, A. Khan, B. Knapmeyer-Endrun, J. Li, R. Maguire, W. T. Pike, H. Samuel, M. Schimmel, N. C. Schmerr, S. C. Stähler, E. Stutzmann, M. Wieczorek, Z. Xu, A. Batov, E. Bozdag, N. Dahmen, P. Davis, T. Gudkova, A. Horleston, Q. Huang, T. Kawamura, S. D. King, S. M. McLennan, F. Nimmo, M. Plasman, A. C. Plesa, I. E. Stepanova, E. Weidner, G. Zenhäusern, I. J. Daubar, B. Fernando, R. F. Garcia, L. V. Posiolova, and M. P. Panning. Surface waves and crustal structure on mars. *Science*, 378(6618):417–421, 2022. URL: `https://www.science.org/doi/abs/10.1126/science.abq7157`, `arXiv:https://www.science.org/doi/pdf/10.1126/science.abq7157`, `doi:10.1126/science.abq7157`.

[24] E. L. Scheller, B. L. Ehlmann, Renyu Hu, D. J. Adams, and Y. L. Yung. Long-term drying of mars by sequestration of ocean-scale volumes of water in the crust. *Science*, 372(6537):56–62, 2021. URL: `https://www.science.org/doi/abs/10.1126/science.abc7717`, `arXiv:https://www.science.org/doi/pdf/10.1126/science.abc7717`, `doi:10.1126/science.abc7717`.

[25] Conway B. Leovy and Richard W. Zurek. Thermal tides and martian dust storms: Direct evidence for coupling. *Journal of Geophysical Research: Solid Earth*, 84(B6):2956–2968, 1979. URL: `https://agupubs.onlinelibrary.wiley.com/doi/abs/10.1029/JB084iB06p02956`, `arXiv:https://agupubs.onlinelibrary.wiley.com/doi/pdf/10.1029/JB084iB06p02956`, `doi:https://doi.org/10.1029/JB084iB06p02956`.

[26] L. R. Dartnell, L. Desorgher, J. M. Ward, and A. J. Coates. Modelling the surface and subsurface martian radiation environment: Implications for astrobiology. *Geophysical Research Letters*, 34(2), 2007. URL: `https://agupubs.onlinelibrary.wiley.com/doi/abs/10.1029/2006GL027494`, `arXiv:https://agupubs.onlinelibrary.wiley.com/doi/pdf/10.1029/2006GL027494`, `doi:https://doi.org/10.1029/2006GL027494`.

[27] Janice Huff, Lisa Carnell, Steve Blattnig, Lori Chappell, George Kerry, Sarah Lumpkins, Lisa Simonsen, Tony Slaba, and Charles Werneth. Evidence report: risk of radiation carcinogenesis. NASA Technical Report SP-2016-6105, NASA Human Research Program, 2016.

[28] Harry J Llamas, Karen L Aplin, and Lucy Berthoud. Effectiveness of martian regolith as a radiation shield. *Planetary and Space Science*, 218:105517, 2022.

[29] Jancy C McPhee and John B Charles. *Human health and performance risks of space exploration missions: evidence reviewed by the NASA human research program*, volume 3405. US National Aeronautics & Space Administration, 2009.

Appendix A. Pictures and 3D models

Figure A.11: Each pixel is obtained by combining the different images. A different location gives an angle of view different, the 3D model is obtained by combining all the images.

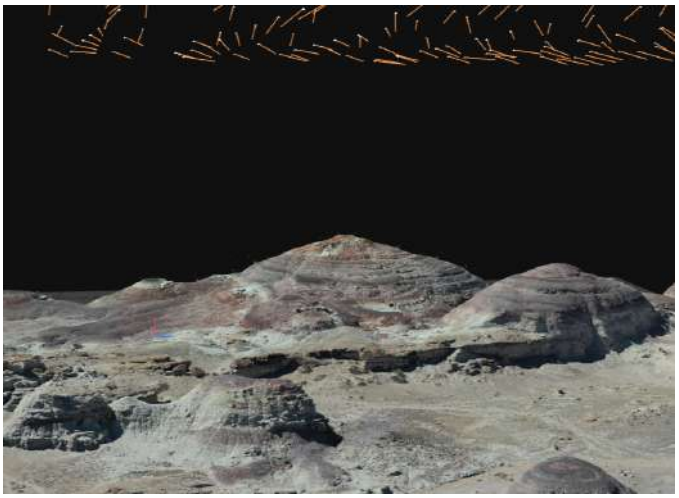

Figure A.12: Point cloud reconstructed by RealityCapture. The position and direction of the aerial images are visible in orange. The region scanned is the Marble Ritual region (38.4036° N, 110.7883° W).

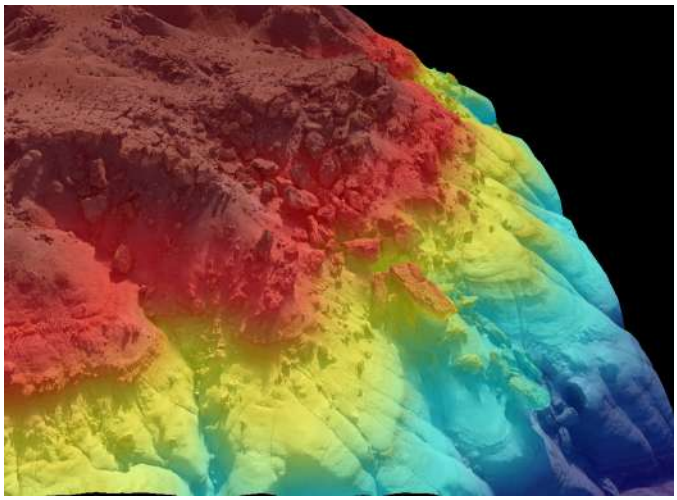

Figure A.13: Elevation of the North Ridge region's model (38.4137° N, 110.7886° W).

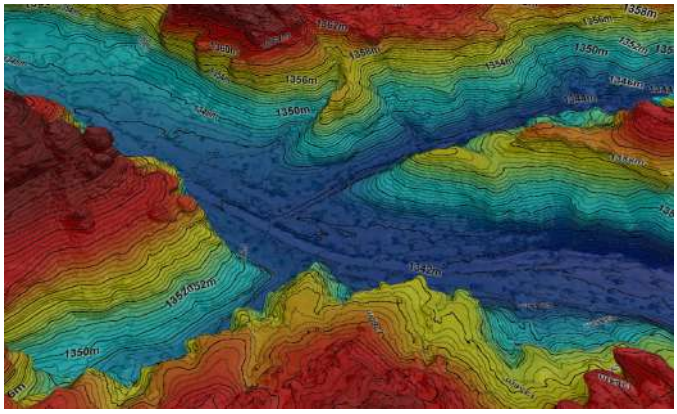

Figure A.14: Topographical model of Candor Chasma (38.4078° N, 110.7651° W).

Figure A.15: Mars Desert Research Station reconstructed by photogrammetry.

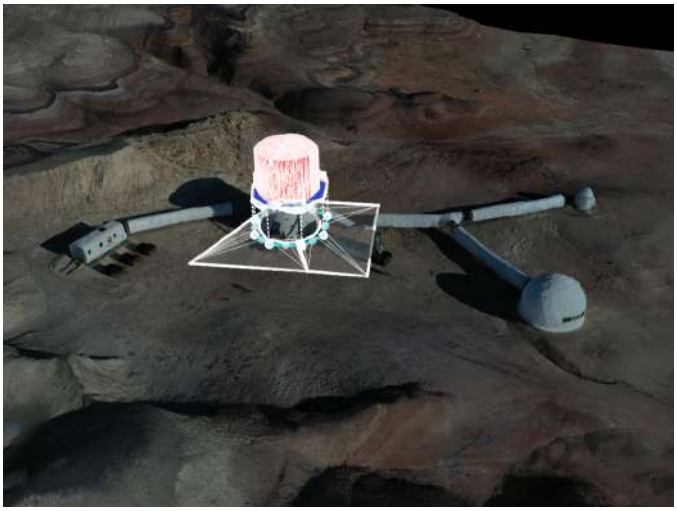

Figure A.16: Volume measurement of the MDRS main module using DroneDeploy tool. The volume above the white surface has been flattened for better accuracy. The volume is around 330 m^3.

Figure A.17: Drone pictures of the skylight caves found in the Kissing Camel Ridge region.

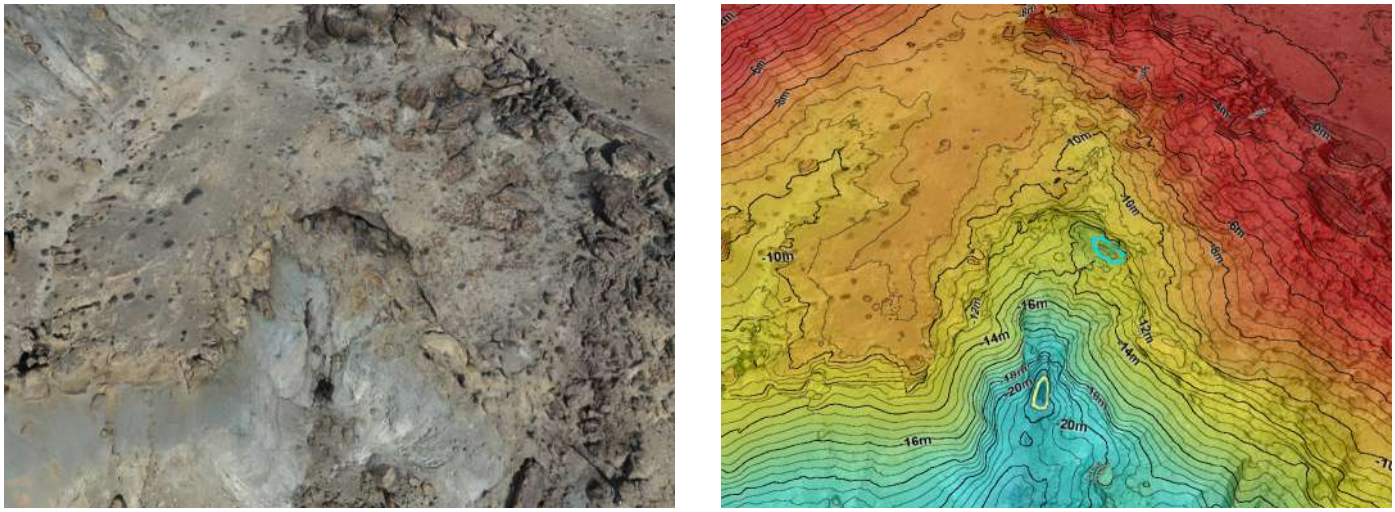

Figure A.18: Skylight-like caves found in the Kissing Camel Rigde region, in blue and yellow.

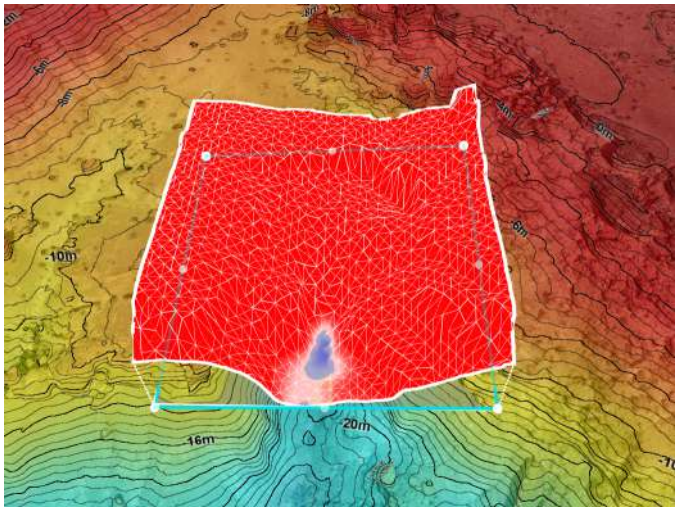

Figure A.19: Volume measurement of the first cave entrance, in blue. In the 3D model, the volume entrance is of 6.85 m^3.

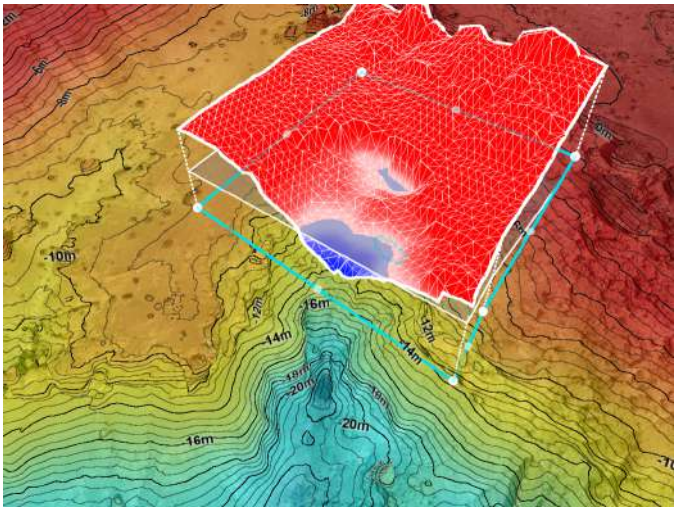

Figure A.20: Volume measurement of the surrounding material above the second entry altitude, in red. It gives approximately 4801 m^3.

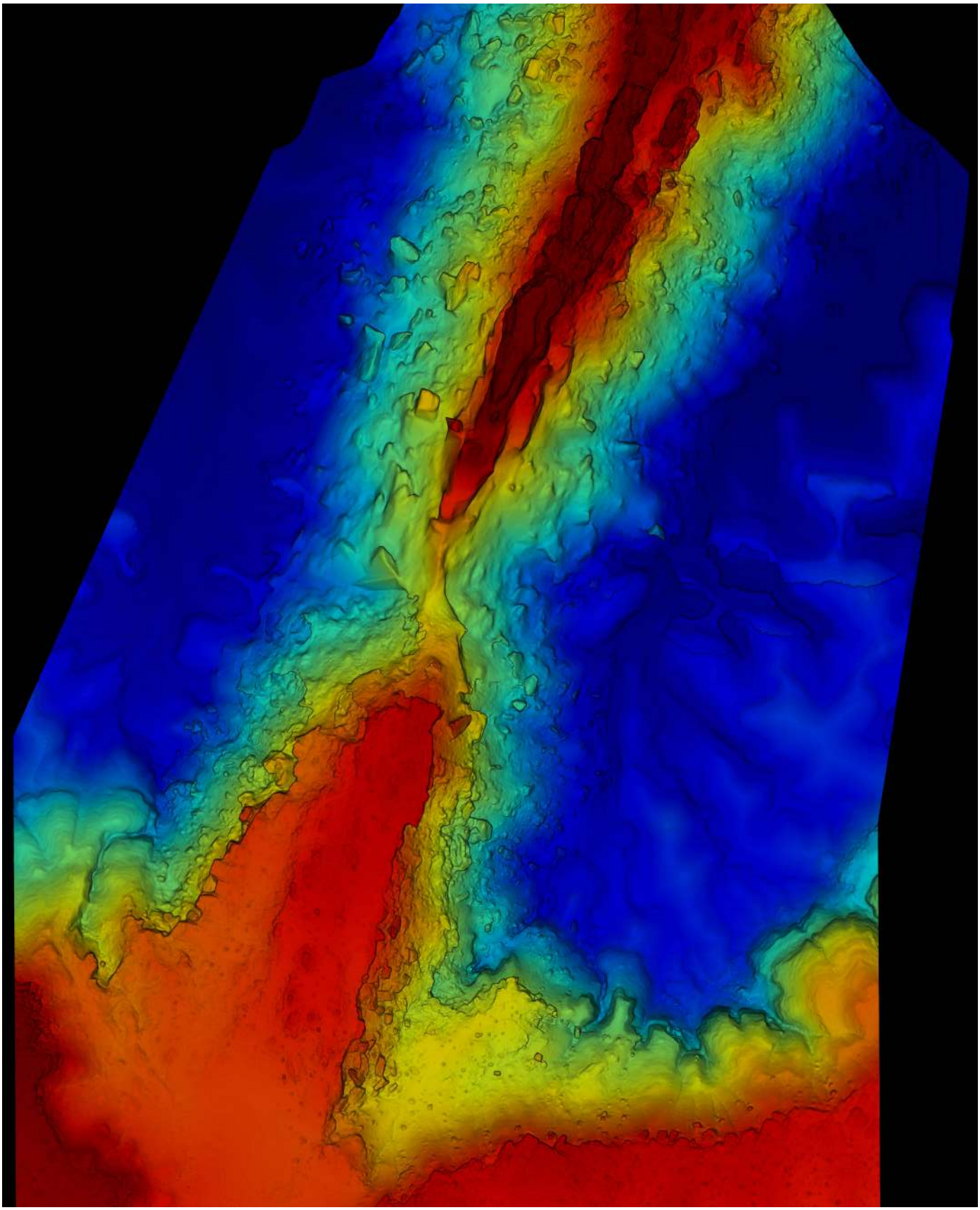

Figure A.21: Topography of Kissing Camel Ridge Region in the Utah Desert (38.3944° N, 110.7952° W). The highest altitudes are shown in red, with a maximum around 1390 m, while the lowest altitudes are shown in blue, with a minimum around 1360 m. The north is oriented towards the left of the page.

Figure A.22: Drone pictures of the Lith Canyon.

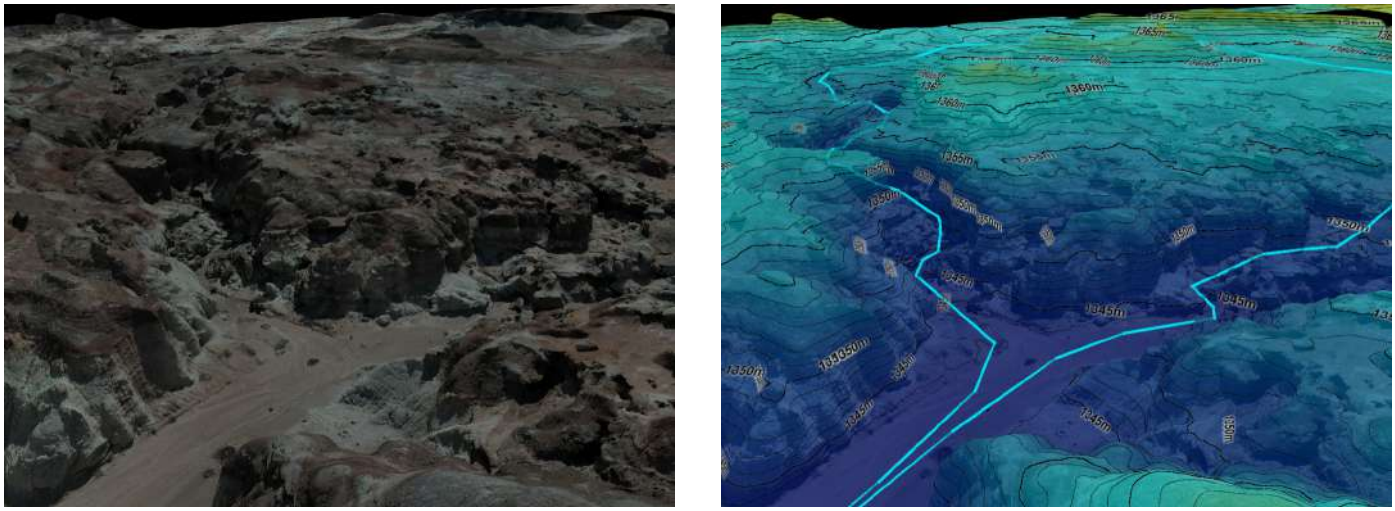

Figure A.23: Lith Canyon identified as the lowest altitude destination, after detection of an incoming CME. Two possible paths to reach the Canyon are represented in the right figure.

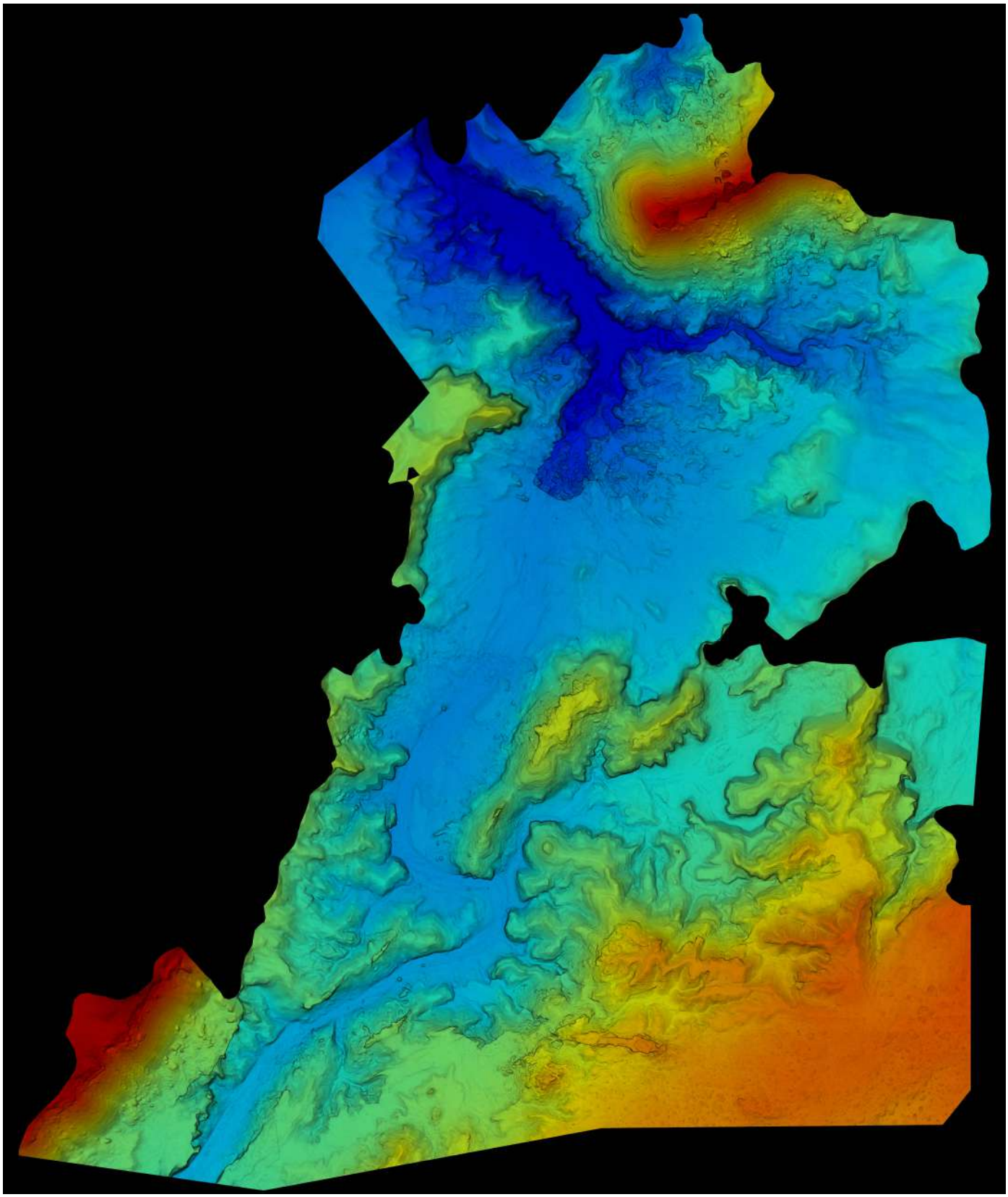

Figure A.24: Elevation of the Special Region in the Utah Desert (38.4563° N, 110.7895° W). The highest altitudes are shown in red, with a maximum around 1395 m, while the lowest altitudes are shown in blue, with a minimum around 1345 m. The north is oriented towards the top of the page.

Figure A.25: Drone pictures of the water area identified around Monte Tharsis.

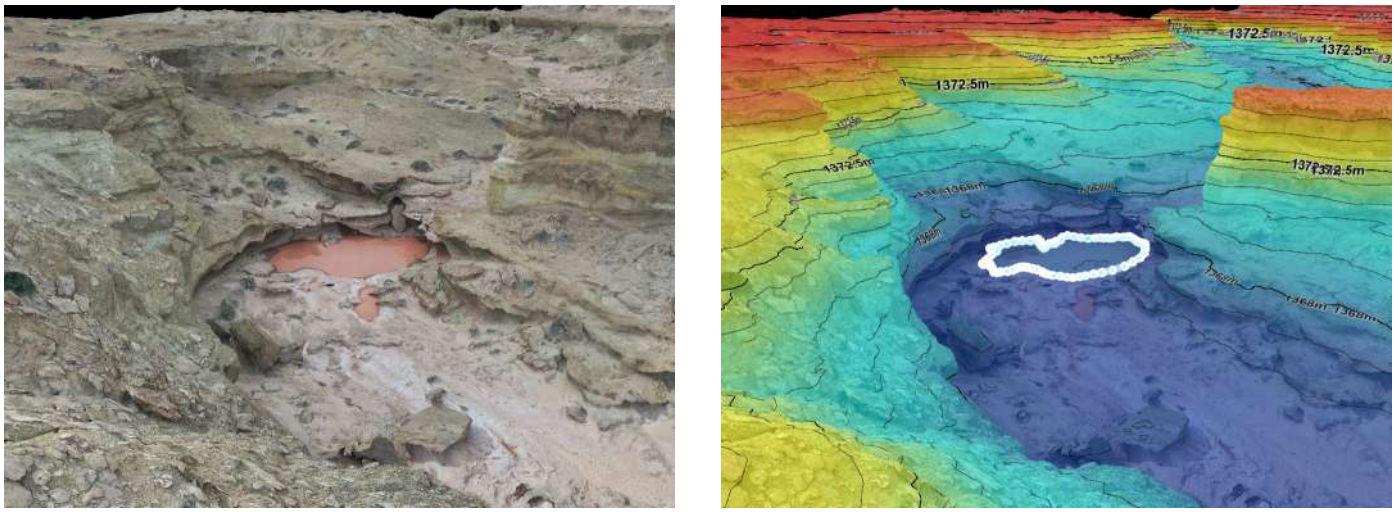

Figure A.26: Water surface mapped during EVA#10. In the right figure, the water surface is estimated to 53.66 m^2.

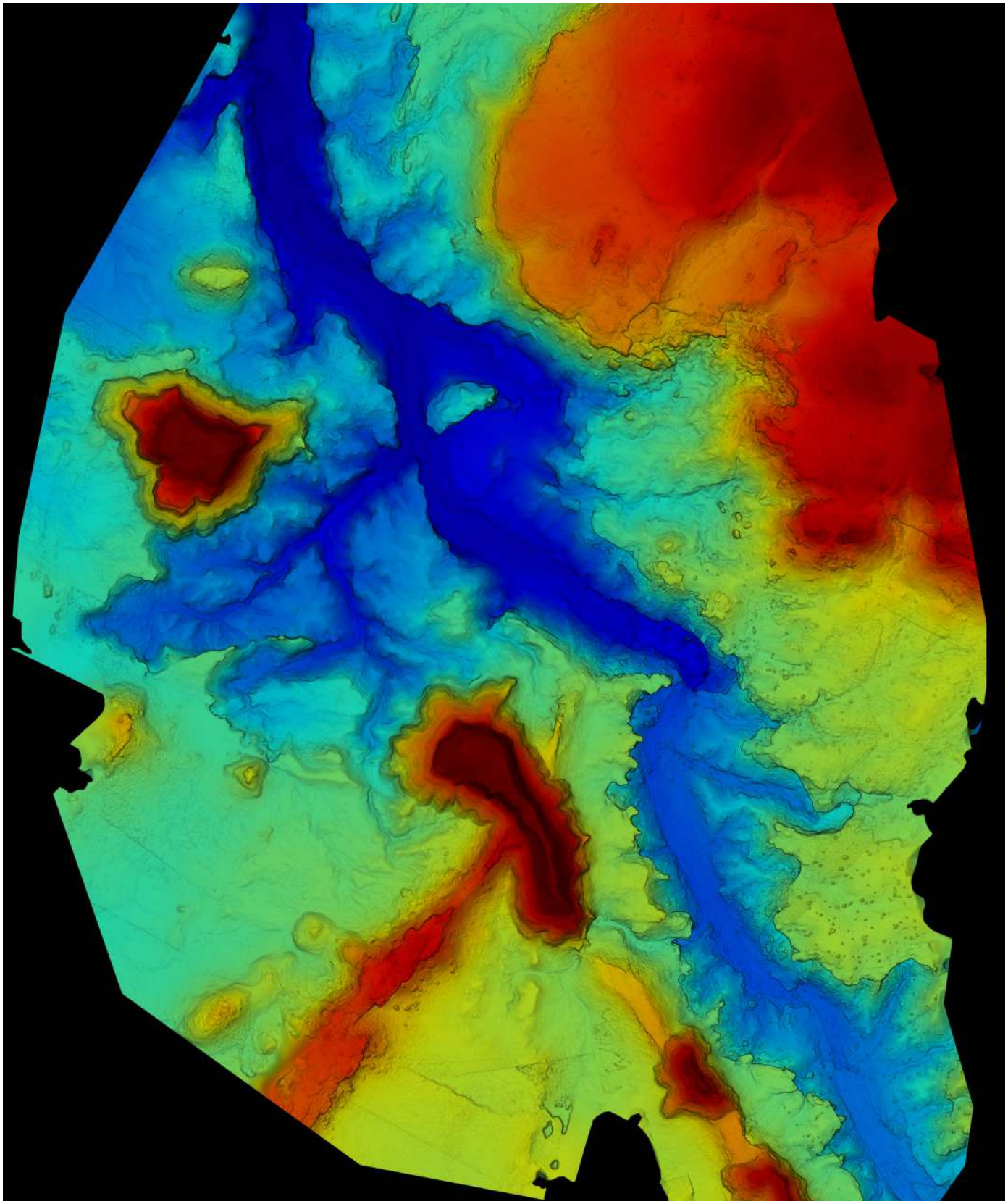

Figure A.27: Elevation around Monte Tharsis in the Utah Desert (38.4269° N, 110.7838° W). The higher altitudes are shown in red, with a maximum around 1380 m, while the lower altitudes are shown in blue, with a minimum around 1365 m. The north is oriented towards the top of the page.